International Journal of Applied Mathematics
& Statistical Sciences (IJAMSS)
ISSN (P): 2319–3972; ISSN (E): 2319–3980
Vol. 11, Issue 1, Jan–Jun 2022; 33–50

International Academy of Science,
Engineering and Technology
Connecting Researchers; Nurturing Innovations

COMPARATIVE STUDY OF DIFFERENT MULTIFRACTAL MOMENTS IN THE SPECTRUM OF PRODUCED PARTICLES IN ^{32}S–AG/BR INTERACTION AT 200 A GEV/*C*

Dr. Malay Kumar Ghosh

Assistant Professor, Department of Physics, S. R. Fatepuria College, Murshidabad, West Bengal, India

ABSTRACT

The fractal nature of non-statistical fluctuations in the density distribution of singly charged particles produced in ^{32}S–Ag/Br interactions at an incident momentum of 200 A GeV/c has been investigated under the frame work of Hwa's multifractal moments, Takagi's Multifractal moments and multifractal detrended fluctuation (MDFA) analysis. The experimental data have been collected by using the nuclear photographic emulsion technique. All results obtained experimental data is analyzed and have been compared with the simulated results.

KEYWORDS: *Nucleus-Nucleus Collision, Fluctuations, Long Range Correlation, Multifractal Moments*

Article History

Received: *29 Apr 2022* **|** ***Revised:*** *02 May 2022* **|** ***Accepted:*** *12 May 2022*

1. INTRODUCTION

As the size of the experimental data is finite there must be present fluctuation in the distribution of produced particle spectrum in high energy heavy ion collision (AB collision) which is statistical in nature. But along with this there also exists another type of fluctuation which arises due to some dynamical reasons. By taking an average over a comparatively large sample the statistical fluctuation may be minimized by a substantial amount. At the time of averaging, the dynamical components are also averaged out, as a result in the final state the distribution become smooth. There exist many statistical techniques by the use of which one may obtain information about the physics of the dynamical nature of the fluctuation present in the distribution of produced particle spectrum. In this field it is well known that the density fluctuation has self-similar multifractal properties which may have resulted due to some kind of scale invariant dynamics. Evaluating appropriate moments of the distribution and by examining how they depend on the phase-space interval size $(¢X)$ one can draw information about the nature of the dynamical fluctuation. According to the theory [1–3] and from the experimental results [4–8], it is established that the self-similarity in density fluctuations should lead to a power-law scaling behaviour of the $¢X$ -dependence of multiplicity moments. Such scaling laws can further be utilized to extract universal fractal properties of the underlying distribution and its fluctuation. Efforts have been made to interpret the observed scale invariances in terms of the random cascading model, phase transition or more conventional phenomenon such as the Bose–Einstein correlation, but each with limited degree of success. Both the experimental and phenomenological status of the subject has been comprehensively reviewed in [9].

The self-similarity of scaled factorial moment (SFM) or intermittency phenomenon is observed in our previous investigation [10]. We observed that in pseudorapidity (¦) space the SFM (F_q) of order q has been found to obey a scaling property like

$$F_q \propto ¢X^{-¤_q}, \quad (1)$$

For a region q=2 to q=6, where $¤_q$ is known as intermittency index. Our previous investigation [10] established that the self-similarity of density fluctuations in one- dimensional particle distribution down to the experimental resolution involves the fractal structures. In the paper [10] we already presented a detail and systematic investigations under the frame work of Hwa's multifractal moments and Takagi's moments and measure the different fractal dimensions. Hence, in this paper I have presented some results on scaling behaviour of multifractal moments as functions of $¢X$, and has been examined by using the different techniques [1, 11- 15]. All the techniques have been described shortly in the methodology section. Results obtained from these three different formalisms of multifractal analysis have been compared to the extent possible. ^{32}S–A/Br events at the same incident momentum and having identical multiplicity distribution as the experimental one have been simulated by using the computer code FRITIOF based on the Lund Monte Carlo model [16]. It is used to compare experimental in case of first two techniques. In order to compare the experimental results in case of third technique I prepared an identical set of simulated data obtained from UrQMD code [16] as experimental one and compare the experimental results with the simulated results. The major objectives of this paper are to establish the presence of multifractal characteristics of the experimental data on density fluctuations beyond those arising from statistical noise in terms of MFDFA moments, and compare all the results obtained from first two techniques how far they agree with each other as well as to extract relevant fractal parameters.

2. EXPERIMENT AND DATA

Nuclear photographic emulsion plates (Ilford G5) were irradiated horizontally with a beam of ^{32}S nuclei at an incident momentum of 200 A GeV/*c* obtained from the super proton synchrotron (SPS) at CERN. After development, washing, mounting on glass plates, and drying, the emulsion plates were volume scanned with the help of Leitz Metalloplan microscopes at a total magnification of 300×. For minimize the error and biasness the scanning was done by two independent observers. Considering a primary interaction induced by the incoming ^{32}S projectile the total number of track of secondary emission was counted and the emission angle (¯) and the azimuthal angle (¤) of each secondary track with respect to the incident projectile track the number of secondary tracks were measured by an oil immersion objectives at a total magnification of 1500×. According to emulsion terminology, the tracks coming out of an interaction can be classified into four categories, namely, shower, grey, black tracks and projectile fragments. The singly charged particles moving at relativistic speed (≈ 0.7) is known as shower track. The particles produced in a high-energy interaction (mostly charged mesons) fall into this category, and the total number of such particles in an event is denoted by n_s. The grey tracks are mainly due to protons knocked out from the target nucleus that directly participate in the interactions. A few percentages of them may also be due to slowly moving mesons. The slowly moving heavy target fragments that coming out of the target nucleus after the interaction has taken place is termed as black tracks. The projectile fragments are the spectator parts of the incoming projectile nucleus. Details of the event selection criteria, classification of tracks and other aspects of the experiment can be found elsewhere [17]. The number of heavy tracks in an event (n_h) is equal to the sum of the number of

black (n_b) and grey tracks (n_g). A cut on the number of these heavy target fragments e.g., $n_h \geq 8$ in each event ensured that a subsample of ^{32}S-interactions only with Ag or Br nuclei has been considered. Here I consider only those interactions for which the number of spectator projectile fragments in an event (n_{pf}) with charge $Z \geq 2$ is equal to zero, which enables us to choose only those interactions for which total fragmentation of the incident ^{32}S nucleus has taken place. Following these criteria, only 200 central and semi-central ^{32}S–Ag/Br interactions was selected for further analysis. The average number of shower tracks for the considered sample of events was, $< n_s >= 217.79 \pm 6.16$, and the present analysis is confined only to the shower tracks.

The rapidity variable, defined as

$$y = \frac{1}{2}\ln\frac{E + p_l}{E - p_l},$$

Is additive in nature under Lorentz transformations and is used to locate a particle in a one-dimensional phase space. Here E and p_l are, respectively, the energy and longitudinal component of linear momentum of the particle. As energy and momentum of the emitted particles is very difficult to measure in case of emulsion experiment it is convenient to replace the rapidity variable by the pseudorapidity variable, as

$$\eta = -\ln\tan\frac{\theta}{2}.$$

Here in comparison with the total energy the rest energy of a particle was neglected, as is the case for most of the charged mesons produced in high-energy interactions. There are many limitations in Nuclear emulsion experiments but it is superior to other experiments in one respect that here we may get a very high angular resolution $(\approx 1 mrad)$, and this advantage can be exploited, where distribution of particles in small phase-space region is to be analysed. To overcome the problem of shape dependence of the emitted particle distribution one can replace the phase-space variable (say η) with a cumulative variable I_η [19] defined as

$$I_\eta = \frac{\int_{\eta_{min}}^{\eta} \rho(\eta)\, d\eta}{\int_{\eta_{min}}^{\eta_{max}} \rho(\eta)\, d\eta}.$$

Here, η_{min} and η_{max} are the minimum and maximum value of η, and $\rho(\eta)$ is the single-particle density distribution in terms of η. Irrespective of the basic phase-space variable from which it is derived, density distribution in terms of the cumulative variable is always uniform in between $I = 0$ and $I = 1$. Though the entire analysis on multiplicity moments will henceforth be preformed taking I_η as the basic variable, we shall continue to call the corresponding space as η-space. The pseudorapidity density distribution $\rho(\eta) = N_{ev}^{-1}(\frac{dn_s}{d\eta})$, for the shower tracks was obtained, $N_{ev}(= 200)$ being the total number of events in our sample. The distribution of $\rho(\eta)$ is well represented by a Gaussian distribution. As

mentioned earlier, the experimental results have also been compared with those obtained by analysing events generated with the computer code FRITIOF based on Lund Monte Carlo model [21] for high-energy AB interaction in case of Hwa's multifractal moments and Takagi's multifractal moments and in case of MFDFA moments we used UrQMD code [16]for simulated data.

3. METHODOLOGY AND RESULTS

3.1 Hwa's Multifractal Moments

It is well known that with the help of fractal geometry it is possible to characterize the distribution and it is well observed in the investigation from the intermittency analysis of the present set of data [10]. According to the theory of multifractality the density of final state hadrons should follow a scaling property with the phase-space partition size, and the scaling properties should be different in different regions of phase space.

Due to the finiteness of average shower track multiplicity $< n_s >$ multiparticle production phenomenon in high energy nucleus-nucleus collision suffers an acute problem. The statistical fluctuation is very large for finite $< n_s >$ of the frequency distribution and its moments. As the bin size gets smaller, the problem of statistical noise arising out of the growing presence of empty bins also requires special attention. The multifractal moment (G-moment) of order *q*, also known as frequency moment, was introduced for an event as [11]

$$G_q = \sum_{j=1}^{M} [\frac{n_{ij}}{(n_s)_i}]^q \Theta(n_{ij} - q) \tag{2}$$

Here *M* is the total number of intervals into which the entire phase space has been divided, n_{ij} is the number of particles in the j^{th} bin of i^{th} event, $(n_s)_i$ is the total number of particles in the i^{th} event, $[(n_s)_i = \sum_{j=1}^{M} n_{ij}]$, and Θ is a step function for integer as well as fractional *q* as defined in [11]. The step function is taken care of in order to account the effect of empty bin. The theory of fractals demands that a self-similar behaviour in dynamical component should present in the density fluctuation, the G-moments should exhibit following scaling behaviour:

$$G_q(\delta_{i\,j}) \propto (\delta_{i\,j})^{\tau(q)} : \quad \delta_{i\,j} \to 0 . \tag{3}$$

Here *τ(q)* is called the mass exponent. The fractal behaviour cannot be extracted in the strict sense as the partition number *M* remains finite, as the limit $\delta_{i\,j} \to 0$ cannot actually be reached and. But one can still obtain significant results by examining the scaling properties of the G-moments in a region where $\delta_{i\,j}$ is of the order of the phase-space resolution permitted by the experiment. Taking the vertical average of G-moments over the sample of events under consideration, one can determine the event space average of mass exponent as

$$< \tau(q) >= -\frac{\partial(< \ln G_q >)}{\partial(\ln M)} \tag{4}$$

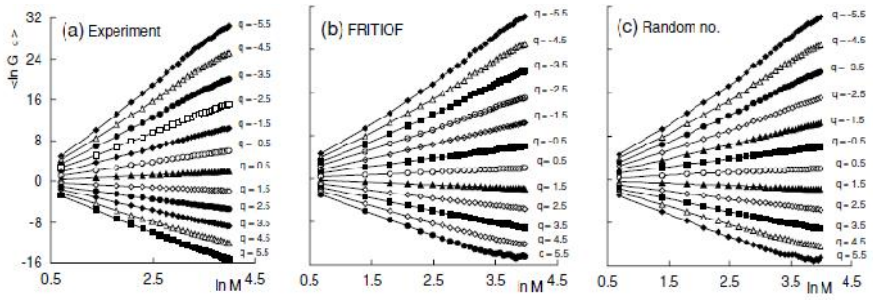

Figure 1: Variation of G-Moments with Phase-Space Partition Number for ^{32}S–Ag/Br Interaction at 200 A GeV/*c*: (a) Experiment, (b) FRITIOF and (c) Random Number. In all Diagrams the Continuous Lines are Drawn Simply by Joining the Points.

In the papers [1, 2 & 11] give a systematic and brief descriptions to determine various parameters related to multifractal characteristics of density fluctuation. For different q Values of <lnG_q > have been plotted against ln$M$ in Fig 1. The experimental results, the FRITIOF simulated results as well as the results obtained by random number generation are shown in the diagram separately. From the above graph, it is very clear that for all three sets of data <lnG_q > linearly depend on ln$M$ in accordance with equation (3), increasing for q < 0 and decreasing for q > 1showing a saturation effect in the large ln$M$ region. This saturation effect is may arise due to finiteness of $< n_s >$.

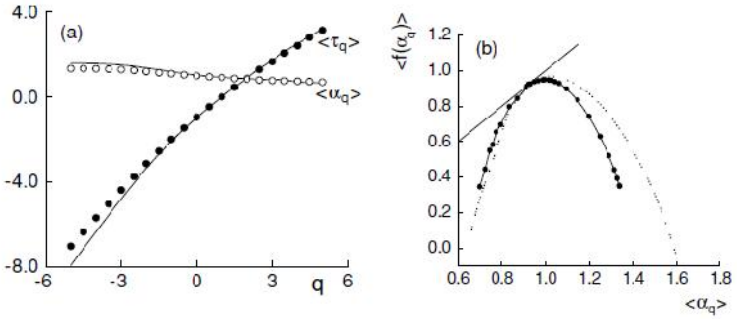

Figure 2: (a) Event Averaged Mass Exponents <*τ(q)*> and Lipschitz–Holder Exponents <α_q > Against q for ^{32}S–Ag/Br interaction at 200 A GeV/*c*. Data Points Represent the Experimental Values and the Lines Represent the Corresponding FRITIOF Predictions. (b) Multifractal Spectral Function for both the Experiment and FRITIOF. The Solid Curve with Points Represents Experimental Results and the Dotted Curve Represents the FRITIOF Prediction. The Straight Line is the $< f(\sim_q) >=< \sim_q >$ Line.

Following equation (4) the <*τ(q)*> values can be determined for each q from the best linear fit of the ln$M$ dependence of <lnG_q >. The event space averaged multifractal spectral function

$$< f(\sim_q) >= q < \sim_q > - < ^2_q >,$$

Is introduced through a Legendre transform with the help of Lipschitz–Holder exponent α_q , that is defined as

$$< \sim_q >= \frac{\partial < ^2_q >}{\partial q}$$

Since a derivative is involved, it is necessary to determine $<\alpha_q>$ for small incremental changes in q, especially in the neighbourhood of $q = 0$, where $<f(\alpha_q)>$ has its maximum. Fig 2(a) shows the variation of $<\tau_q>$ and $<\alpha_q>$ values for the experimental and FRITIOF data with q. Here no such significant difference is found between the experimental and simulated results which are contradictory to the case of intermittency analysis [10]. A smooth and stable multifractal spectral function $<f(\alpha_q)>$ has been obtained both for the experiment and for the FRITIOF. Multifractal spectral function $<f(\alpha_q)>$ for both experiment and simulated data are plotted against $<\alpha_q>$ in Fig 2(b), and both satisfy the general characteristics mentioned in [1, 3] such as (i) $<f(\alpha_q)>$ is a function of $<\alpha_q>$ that is concave downwards, (ii) has a peak at $<\alpha_0>$, and (iii) the straight line $<f(\alpha_q)> = <\alpha_q>$ tangentially touches both the spectra around $<\alpha_1>$, because $<f(\alpha_1)> = <\alpha_1>$ and $<f'(\alpha_1)> = 1$. The region above the $<f(\alpha_q)> = <\alpha_q>$ line has no physical significance and corresponds to an unphysical region. The wide distribution in $<f(\alpha_q)>$ and not a delta function peaked around α_0 observed in the diagram confirms multifractal nature of the density fluctuation in each case. The region of the spectrum where the value of $<\alpha_q>$ less than unity corresponds to the dense region of the spectrum and for the region for which the value of $<\alpha_q>$ is greater than unity is corresponds the sparse region of density distribution. Both experimental and simulated maximum values of $<f(\alpha_q)>$ are very close to unity, indicating that the empty bin effect particularly in the higher resolution region is marginal in the present case. The FRITIOF simulated spectrum is wider than the experimental one. We already know for a *pp* interaction a similar feature has been observed while UA1 data were being compared with GENCL and PYTHIA predictions [4]. In the case of *AB* interactions multifractal characteristics were observed both in the experimental data as well as in the Monte Carlo predictions based on a simple stochastic model [8].

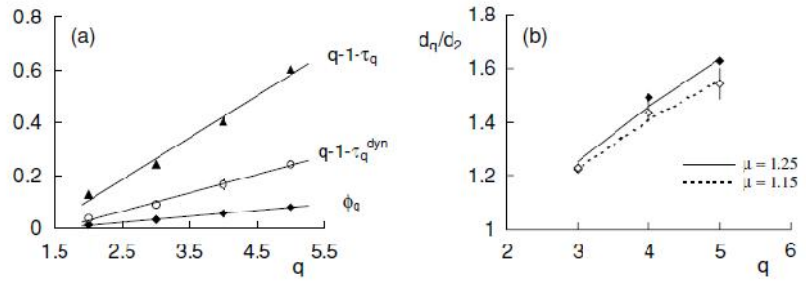

Figure 3: (a) Experimental Values of the Intermittency Indices (φ_q), $(q - 1 - <\tau(q)>)$ and $(q - 1 - <\tau(q)>^{dyn})$ are Plotted Against q for ^{32}S–Ag/Br Interaction at 200 A GeV/c. The Straight Lines are best Linear fit to data. (b) Experimental Values of d_q/d_2 Obtained both from SFM (Solid Diamonds) and G-Moments (Open Diamonds) are Plotted Against q. The Continuous (Solid and dotted) Lines Represent the Corresponding Levy Law Prediction using Equation (9).

For the finiteness of the average number of charged particle, the G_q moments contain statistical contribution (G_q^{st}), this statistical part can be determined by distributing *ns* particles of an event randomly within $0 \leq \text{¡}_i \leq 1$. It should be remember that in this process short-range correlation among the particles, if any, is destroyed. The dynamical contribution (G_q^{dyn}) can then be extracted after eliminating the statistical one. In [11] it has been shown that, for a trivial dynamics the dynamical part of $<\tau_q>$, denoted by $<\tau(q)>^{dyn}$, should be equal to $(q - 1)$. The deviation in $<\tau(q)>^{dyn}$ from $(q - 1)$ is from the nontrivial dynamical contribution. As all three G-moments G_q, G_q^{st} and G_q^{dyn} obey their respective power laws, the following relation may be obtained:

$$<^2(q)>^{dyn} = <^2(q)> - <^2(q)>^{st} + q - 1 \qquad (5)$$

whereas, the intermittency index φ_q introduced in equation (1), can also be connected to $\langle\tau(q)\rangle^{dyn}$ as [11]

$$\langle ²(q)\rangle^{dyn} - q + 1 \approx ¤_q . \tag{6}$$

In Figure 3(a) the variation of φ_q values along with the ($q - 1 - \langle\tau(q)\rangle$) and ($q - 1 - \langle\tau(q)\rangle^{dyn}$) values against q is shown. From the diagram it is clear that the φ_q values differ from the respective ($q - 1 - \langle\tau(q)\rangle^{dyn}$) values by very small amount. The difference in their values may probably be attributed to the different ways of defining SFM and G-moment. The generalized Renyi dimensions, denoted by D_q , may be obtained from the intermittency indices as

$$D_q = 1 - \frac{¤_q}{q-1} \tag{7}$$

Therefore, with the help of equation (6) one can demand

$$D_q \approx \frac{\langle ²(q)\rangle^{dyn}}{q-1} . \tag{8}$$

Simultaneously the anomalous dimensions are defined as

$$d_q = D - D_q .$$

Where, D is the topological dimension of the supporting space. D = 1stands for the one dimensional analysis. The Levy index (μ) is a very useful parameter to classify the properties of universal multifractals. For multifractal nature it is found that the value of μ is lying between $0<\mu< 2$. Levy index indicates the degree of multifractality as well as estimates the cascading rate in self-similar branching process [16]. The Levy index (μ) can also be utilized to highlight the possible mechanism of particle production. Such a characterization of multifractality is possible if the underlying density distribution can be described by a Levy stable law. Under a Levy law approximation, using anomalous dimensions one can determine the value of μ from the following relation [21]:

$$\frac{d_q}{d_2} = \frac{1}{2^{«} - 2}\frac{q^{«} - q}{q-1} \tag{9}$$

In Figure 3 b. Experimental values of d_q/d_2 obtained both from SFM (solid diamonds) and G-moments (open diamonds) are plotted against q. The lines correspond, respectively, to μ = 1.15 for the exact values of φ_q and to μ = 1.25 for the approximate values. If μ were equal to 2, the Levy distribution would have transformed into a Gaussian one. Minimum fluctuation in the self-similar branching processes is expected under such condition. On the other hand, the value of $dq/d2$ become independent of order for μ = 0. This condition corresponds to mono-fractals and maximum fluctuation. Under such condition one may expect a second-order phase transition. In our case neither of the above two conditions is satisfied by the μ values obtained. One can see that the present values obtained from two different sets of parameters, are very close to each other. The fact that μ >1.0, demands the presence of wild type of singularities arising out of fluctuations in the density distribution which is non-Poisson like in nature. Here, it can be concluded as the mechanism of particle production in the present case of ^{32}S–Ag/Br interactions may be described in terms of a possible non-thermal phase transition during the cascading process. On the other hand, a value of 0 < μ < 1.0 would have indicated soft bound singularities, that can be related to a thermal phase transition interspersed in the cascading process. It should however be mentioned that the present values of Levy index are less than a previously obtained value (μ = 1.6) based on a set of

combined data on *AB*, *pA*, e+e− and *μp* interactions [21], but are well within the limit allowed by the Levy law description, and do not necessarily warrant a thermal phase transition to occur during particle production.

3.2 Takagi's Multifractal Moments

In order to overcome the difficulties of finiteness of the number of charged particle multiplicity an alternative approach has suggested by Takagi [12]. According to his methodology a new set of multiplicity moments for $q > 0$ are suggested as

$$T_q(¢i_{¦}) = \ln \sum_{i=1}^{N_{ev}} \sum_{j=1}^{M} (p_{ij})^q \tag{10}$$

T_q is known as Takagi's multifractal moments and are not affected by the finiteness of n_s. Here, *pij (= nij /K)* is the normalized density function, *K* is the total number of particles produced in *Nev* interactions and *nij* is the same as equation (2). Takagi's method is based on two assumptions, (i) over the considered phase-space interval the density function ρ is uniform, and (ii) the multiplicity distribution *Pn* does not depend on the location of the interval $¢i_{¦}$. The above two conditions are found to be valid in the present case where $X\eta$ has been used as a phase space variable. According to the theory of multifractals, $Tq(¢i_{¦})$ should be a linear function of the logarithm of the resolution $R(¢i_{¦})$ as,

$$T_q(¢i_{¦}) = A_q + B_q \ln R(¢i_{¦}), \tag{11}$$

Where *Aq* and *Bq* are two constants which are independent of *q*. If the linear dependence like that of equation (11) is observed over a large range of $R(¢i_{¦})$, following Takagi's method the generalized dimensions can once again be calculated as -

$$D_q = B_q/(q-1) \tag{12}$$

For $q = 1$, one may either take the appropriate limit [22], or may introduced the entropy function defined as

$$S(¢i_{¦}) = -\sum_{i=1}^{N_{ev}} \sum_{j=1}^{M} p_{ij} \ln p_{ij} \quad . \tag{13}$$

The entropy function is also defined as,

$$S(¢i_{¦}) = -D_1 \ln R(¢i_{¦}) + const., \tag{14}$$

Where, *D*1 is termed as information dimension. If the number of events *Nev* is quite large one will get

$$\sum_{i=1}^{N_{ev}} \sum_{j=1}^{M} (p_{ij})^q = < n_q > /(K_{q-1} < n >) \quad . \tag{15}$$

Where average bin multiplicity $<n> = K/(M.\ Nev)$, and therefore, it can be write

$$\ln n_q = A_q + [(q-1)D_q + 1] \ln(¢i_{¦}) \quad . \tag{16}$$

For the simplest choice of $R(¢i_{¦})$, = $¢i_{¦}$. Replacing $¢i_{¦}$ with $<n>$, the generalized dimensions can now be obtained following the relations:

$$\ln n^q = A_q + [(q-1)D_q + 1]\ln < n > \tag{17}$$

for $q \geq 2$. For $q = 1$,

$$< n \ln n > / < n > = C_1 + D_1 \ln < n > . \tag{18}$$

Proceeding in the same way as [12], for a symmetric interval about the central value $\delta = 0.5$ of the distribution, The values of $<n \ln n>$ and $\ln<nq>$ are calculated with increasing width of the interval about the central value ($\delta = 0.5$) of the distribution according to the procedure mentioned in [12]. Our results on Takagi's method of multifractal analysis have been graphically shown by plotting $<n \ln n>/<n>$ against $\ln<n>$, in Fig 4(a)–(c), respectively for the experimental values in both η and ϕ-space and the FRITIOF prediction in η-space. Similarly the variation of $ln<n^q>$ against $\ln<n>$ is shown in the Fig 4(d)–(f). From the slopes of best linear fit to data values of the plot $<n \ln n>/<n>$ vs $\ln<n>$ the information dimension (D_1) have been calculated respectively as $D_1 = 0.973 \pm 0.0014$, 0.972 ± 0.002 and 0.979 ± 0.002 . Values of generalized dimensions for $q \geq 2$ have been obtained

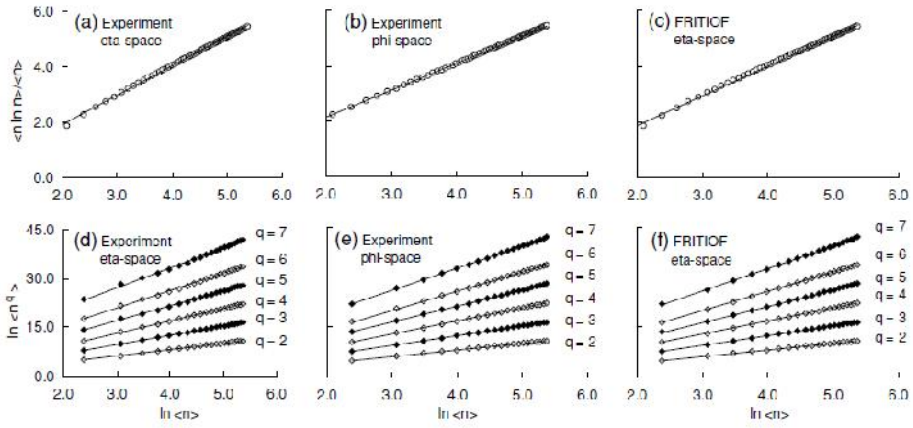

Figure 4: Plot of Takagi's Multifractal Moments for ^{32}S–Ag/Br Interaction at 200 A GeV/c. In all Diagrams the Straight Lines Represent best Linear fit to data

From the best linear fit of $\ln<nq>$ values against $\ln<n>$ as shown in Fig 4(d)–(f). For comparison, Dq values of different orders obtained from Takagi's generalized moments are plotted against $q \geq 2$ in Fig 5, together with those obtained from the intermittency indices (φ_q) and from the dynamical part of Hwa's multifractal mass exponents $<\tau(q)>_{dyn}$, respectively, making use of equations (7) and (8). With increasing q in general we find a monotonous deceasing trend in the Dq values. However, the Dq values from Takagi's method exhibit steepest fall, whereas those obtained from the intermittency indices decrease at the slowest rate. Probably because of the different ways of defining the multifractal T-moments, and due to the reason that in Takagi's method no attempt has been made to separate the nonstatistical contribution from the statistical one, in this case at large q the Dq values differ significantly from those obtained from the SFMs and G-moments. However, for a simple Poissonian multiplicity distribution within a given interval δ , the D_q values would all have been equal to unity. Any deviation in their values from 1.0 would thus provide us with a measure of nonstatistical fluctuation. This has been found in all the methods described above for characterizing multifractality in density fluctuations.

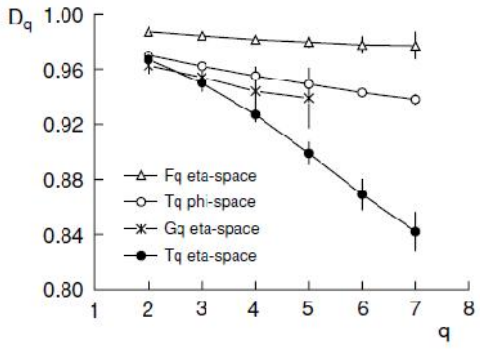

Figure 5: Experimental Values of the Generalized Dimensions D_q for ^{32}S–Ag/Br Interaction at 200 A GeV/*c*. Solid Lines are drawn to Guide the Eye.

On the basis of the fact that only Bernoulli type of fluctuations are responsible for a transition from monofractality to multifractality, Bershadski [23] gave a thermodynamic interpretation of the observed results in terms of a constant specific heat *c*:

$$D_q = D_\infty + \frac{c \ln q}{q-1} \tag{19}$$

A monofractal to multifractal phase transition corresponds to a gap in the value of *c* from *c* = 0 to a nonzero finite multifractal specific heat. By plotting *Dq* against ln *q*/(*q* − 1) we can, therefore, obtain the value of specific heat from the slope of the best linear fit. Such a plot can be found in Fig 6, both for the experiment and FRITIOF simulated values. In ¡ ¦ -space a strict linearity is not seen over the entire range of *q* under consideration, and a linear fit in the range *q* = 2–5 resulted into *c* = 0.329 ± 0.061 ≈ 1/3. On the other hand,

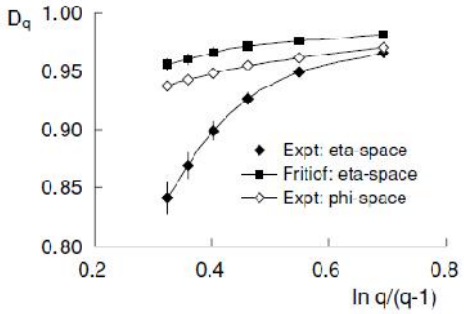

Figure 6: Graph to Determine the Multifractal Specific Heat for ^{32}S–Ag/Br Interaction at 200 A GeV/*c*, from the D_q Values Obtained by using Takagi's Method. The Experimental data Points in *η*-Space are Simply Connected by a Continuous Line, whereas, for both the FRITIOF Prediction in *η*-Space and the Experimental data Points in *ϕ*-Space, the Straight Lines Represent best Linear fit.

best linear fit of FRITIOF data in ¡ ¦ -space over *q* = 2–7 results in *c* = 0.066 ± 0.009, which is much smaller than the corresponding experimental value. On the other hand, in ¡ ¤ -space linear fit once again over the entire range of *q* (= 2–7) gave us a much smaller value of *c* (= 0.086 ± 0.008). The *c*-value in ¡ ¤ -space is significantly smaller than a previously

obtained value (c = 1/4) based on an analysis in the azimuthal angle space of similar ^{32}S-ion induced experiment at same incident energy [24]. As a probable reason for this discrepancy it may be pointed out that the analysis presented in [24] has been performed over a set of events with minimum bias, that possesses a much wider range of impact parameter values, and also has a much smaller value of average shower multiplicity as well as smaller statistics than the present set of experimental data. Here the value of c in ϕ-space is also smaller than the predictions of another analysis (c = 0.56) on simulated high multiplicity single jet events in the azimuthal angle space [25].

3.3 MFDFA Moments

In many cases the local singularities of particle density functions $\circ(\text{¢}X)$ can be described by a power law like,

$$\lim_{\text{¢}X \to 0} \circ(\text{¢}X) \propto (\text{¢}X)^{D_F} \tag{20}$$

and may be interpreted as a self-similar (or self-affine in two dimension) fractal object with dimension D_F . Now each phase-space interval will have its own $\text{¢}X$ dependence. If all of them are characterized by a same D_F, the distribution is considered as a geometrically monofractal object. If the exponent varies at different X positions then it is a multifractal one. The multifractal detrended fluctuation analysis (MF-DFA) has so far not been used extensively for multiparticle emission data analysis [15]. The detrended fluctuation analysis (DFA) method [13] is a very useful technique for the determination of (mono) fractal scaling properties and the detection of long-range correlations in noisy and stationary time series data [14]. Kantelhardt et al. [15] have advanced the DFA method for nonstationary and multifractal series, and the generalized DFA is said to be the multifractal DFA (MF-DFA) method. The DFA and the MF-DFA methods are very standard techniques for the time series data analysis, for completeness we provide a brief description of the methods in the following section. Let x_k: k = 1, 2, . . . , N be a fluctuating series (signal) of length N. The DFA/MF-DFA procedure consists of the following five steps:

Step-1: Determine the Profile

$$Y(i) = \sum_{K=1}^{i} \left[x_K - \langle x \rangle\right], I = 1, 2, \ldots, N \tag{21}$$

Where $\langle x \rangle = \frac{1}{N}\sum_{K=1}^{N} x_K$ is the mean value of the analyzed signals.

Step 2: Determine the Profile

Divide the profile $Y(i)$ into $N_s = \text{int}(N/s)$ non-overlapping segments of equal length s. One has to choose the s value depending upon the signal length. In case, the length N is not a multiple of the considered scale parameter s, the same dividing procedure is repeated starting from the opposite end of the signal. Hence, in order not to disregard any part of the signal series, usually altogether $2N_s$ segments of equal length are obtained.

Step 3: Calculate the local trend for each of the $2N_s$ segments. This is done by least-square fits of the segments (or subseries). Linear, quadratic, cubic or even higher order polynomial may be used to detrend the signal, and accordingly the procedure is said to be the MF-DFA1, MF-DFA2, MF-DFA3, . . . analysis. Let, $y_{\neg}$ be the best fitted polynomial to an arbitrary segment ¬ of the signal. Then determine the variance as

$$F^2(\nu, s) = \frac{1}{2N_s}\sum_{i=1}^{s}\{Y[(\nu-1)s+i] - y_\nu(i)\}^2 \tag{22}$$

For $N = 1, 2, \ldots\ldots N_s$ and $\nu = N_s+1, \ldots\ldots 2N_s$ is given as,

$$F^2(\nu, s) = \frac{1}{s}\sum_{i=1}^{s}\{Y[N-(\nu-N_s)s+i] - y_\nu(i)\}^2 \tag{23}$$

Step 4: The DFA function F is defined by averaging $F^2(\nu, s)$ over all the $2N_s$ segments, i.e.

$$F(s) = \frac{1}{2N_s}\sum_{i=1}^{2N_s}\{F^2(\nu, s)\}^{1/2} \tag{24}$$

On the other hand, the q[th] order MF-DFA function $F_q(s)$ is defined as

$$F(s) = \frac{1}{2N_s}\sum_{i=1}^{2N_s}\{F^2(\nu, s)\}^{q/2}{}^{1/q} \tag{25}$$

for all $q \neq 0$ and for $q = 0$ the above definition is modified to the following form:

$$F(s) = \exp\left\{\frac{1}{4N_s}\sum_{i=1}^{2N_s}\{F^2(\nu, s)\}\right\} \tag{26}$$

In general, the order parameter q can take any real value. Note that for $q = 2$ the MF-DFA function reduces to the standard DFA function as defined in Eqn. (23).

Step 5: Now varying the scale parameter (s), one can study the scaling behaviour of the detrended fluctuation functions. If the signal series x_k possesses long-range (power-law) correlation, $F(s)$ as well as $F_q(s)$ for large values of s would follow a power-law type of scaling relation such as

$$F(s) = s^H \text{ and } F_q(s) \propto s^{h(q)} \tag{27}$$

The exponent H is nothing but the well known Hurst exponent that can be related to the fractal dimension D as: $D=2-H$. According to the value of H, x_k is considered as long-range anti-correlated if 0 < H < 0.5; uncorrelated if H = 0.5 and long-range correlated if $H > 0.5$. On the other hand, the $h(q)$, is termed as the generalized Hurst exponent [15]. For stationery time series $h(q=2) = H$, i.e. the well known Hurst exponent. For a monofractal signal $h(q)$ is independent of q since the variance $F^2(\nu, s)$ is identical for all the subsignals, and hence Eq. (25) yields identical values for all q. Here the function $F_q(s)$ can be defined only for $sm+2$, where m is the order of the detrending polynomial. Moreover, $F_q(s)$ is statistically unstable for very large S(N/4). If small and large fluctuations scale differently, there will be a significant dependence of $h(q)$ on q. Whereas for positive values of q, $F_q(s)$ will be dominated by the large variance which corresponds to the large deviations from the detrending polynomial, for negative values of q major contributions of $F_q(s)$ arise from small fluctuations from the detrending polynomial. Thus for positive (negative) values of q, $F_q(s)$

describes the scaling behaviour of the segment with large (small) fluctuations. Knowing the values of $h(q)$ one can easily estimated the multifractal mass exponent $\tau(q)$ and the multifractal singularity spectrum $f(\alpha)$. It is very well known that the $h(q)$ is related to $\tau(q)$ through

$$\tau(q) = qh(q) - 1 \tag{28}$$

A non linear $\tau(q)$ spectrum demands the existence of multifractal nature of the analyzed time series data. For a monofractal system $\tau(q)$ should be a linear function of q. The singularity strength function $\alpha(q)$ and the multifractal spectrum $f(\alpha)$ are connected via Legendre transformation [26, 27]: $\alpha(q) = \partial\tau_q / \partial q$ as,

$$f(\alpha) = q\alpha - \tau(q) \tag{29}$$

The generalized fractal dimension D_q may be derived from the mass exponent $\tau(q)$ as:

$$D_q = \frac{\tau(q)}{q-1} \tag{30}$$

Here these methods are employed to the single-event η distributions of produced charged mesons in high-energy nucleus-nucleus collisions. The scale parameter s is nothing but the number of partitions in η-space. In Fig. 7, I plot the averaged DFA function $\langle F(s) \rangle$ with phase space partition number (scale) s for the ^{32}S - Ag/Br data. From Fig.1 it is clear that $\langle F(s) \rangle$ for large values of s would follow a power-law type of scaling relation. In this analysis I vary s from *N* to *N/4*, where *N* is the multiplicity cut. In the region $8 \le s \le 24$ the scaling relation (27) holds good. As the scaling behaviour holds well for a fairly large value of s in all cases, one

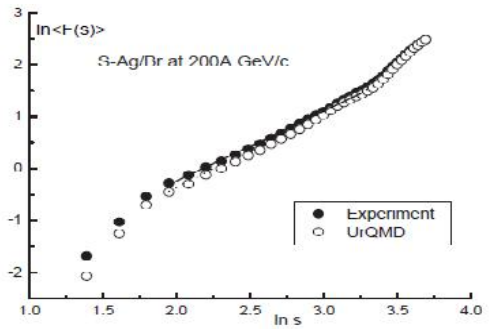

Figure 7: The Variation of Event Averaged DFA Fluctuation Functions $\langle F(s) \rangle$ with Scale Parameters for the ^{32}S - Ag/Br Interaction at 200A GeV/c. The Solid (dotted) lines Represent the best Fitted Straight Lines to the Experimental (UrQMD) data.

May expect that the signal series x_k should possess some kind of long-range (power-law) correlation for both experimental and simulated (UrQMD) data. Here I find that H = 1.474 ± 0.017 (experiment) and H =1.585±0.017 (UrQMD). In all the cases the value of H greater than unity again establish the fact that there must present some long range correlation in both experimental and simulated (UrQMD) data. Using the relation $D_F = 2 - H$, I estimate the values of

fractal dimension (D_F) as D_F = 0.526 ± 0.017 (experiment) and D_F = 0.415 ± 0.017 (UrQMD). It is well known that, for a fractal object the fractal dimension D_F is less than D_T, the topological dimension of the supporting space. For one dimensional analysis the value of D_T = 1. The deviation of D_F from D_T is a measure of the degree of fractality. All the values of D_F obtained from this analysis are much smaller than unity and hence my DFA results demand that the ¦ distributions in the interactions are highly fractal. It is also clear that the UrQMD model possesses fractal dynamics that is apparently identical to those of the experiments. In our previous multifractal analysis using the data of ^{32}S -Ag/Br interaction we observed similar behaviours. All these observations (present and previous) suggest that (multi)fractality gets weakened with increasing multiplicity. In Fig. 8, the variation of event averaged MFDFA fluctuation functions with scale parameter s is shown for both experimental and simulated data.

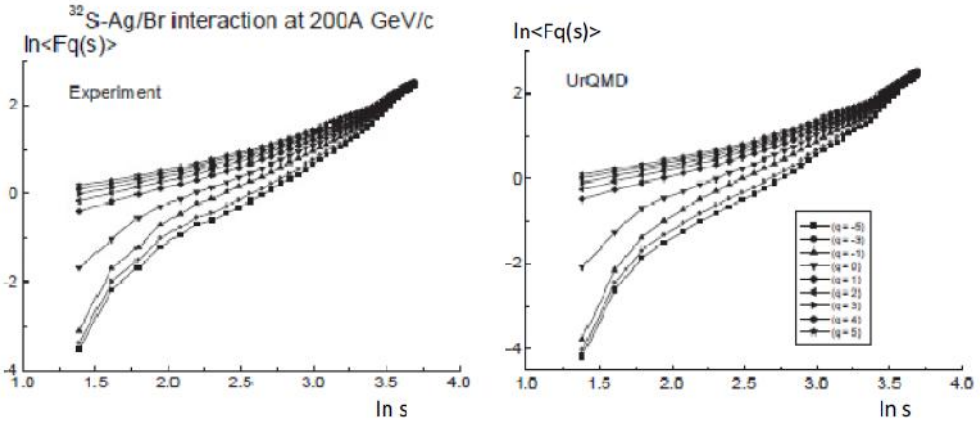

Figure 8: The Variation of Event Averaged MFDFA Fluctuation Functions with Scale Parameter s. Left Panel: Results obtained from Experimental data and Right Panel: Results Obtained from UrQMD data. The Lines Joining Points are shown to Guide the Eye.

From the variation of $< F_q >$ against the scale parameter s it is obvious that there are no saturation effects at higher value of s like G_q moments [10] and hence one may conclude that $< F_q >$ function presented here are not significantly influenced by the finiteness of the event multiplicity. In Fig. 9 the experimental and simulated values of Hurst exponent $h(q)$ for ^{32}S - Ag/Br interaction are plotted against order q. The values of $h(q)$ is determined from the linear portion $4 \le s \le 12$ of $< F_q >$ vs s graph. For $q \le -1$ region the values of $h(q)$ decreases slowly and there is a sharp fall in the q = −1 to q = 1 region and then $h(q)$ tends to saturate in the region $q \ge 1$.

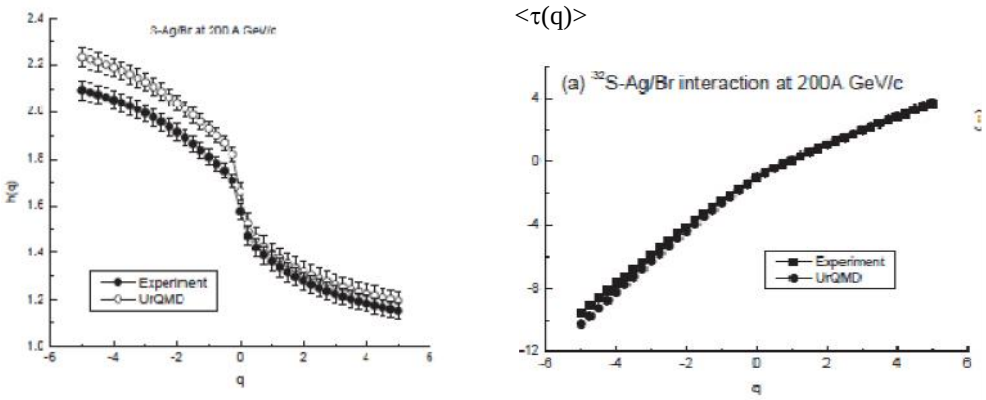

Figure 9: Left Panel: The Variation of Event Averaged h_q Functions with scale Parameter s for ^{32}S - Ag/Br Interaction at 200AGeV/c. The Lines Joining Points are Shown to guide the Eye. Right Panel: The Variation of Event Averaged Mass Exponent $^{2}(q)$ with Scale Parameters for ^{32}S - Ag/Br Interaction

In Fig. 9. I have also graphically represented how the values of $^{2}(q)$ for the experimental and UrQMD data vary with q. Unlike in the case of intermittency analysis, here no significant difference between the experimental and simulated results is observed. Mass exponents $^{2}(q)$ were derived from the fluctuation functions for q values between −5 and +5 and plotted against the q values. A nonlinear $<^{2}(q)>$ function means multiple scaling, which requires a hierarchy of scaling exponents (multiscaling) in order to accurately represent the scaling property. The degree of non-linearity of $<^{2}(q)>$ function can give an idea about the degree of multifractality. These nonlinear functions have convex downward facing plots, with the degree of convexity reflecting the level of heterogeneity in scaling exponents. A smooth and stable multifractal spectral function $f(\sim)$ has been obtained both for the experiment and for the UrQMD for ^{32}S induced interactions. Multifractal spectra are plotted against $\sim$ in Fig. 10, and satisfy the general characteristics [1, 2] such as (i) $f(\sim)$ is a function of $\sim$ that is concave downwards, and (ii) has a peak at $\sim_0$. But unlike the Hwa's multifractal analysis the moments violates the condition (iii) i.e. straight line $f(\sim)=\sim$ tangentially touches both the spectra.

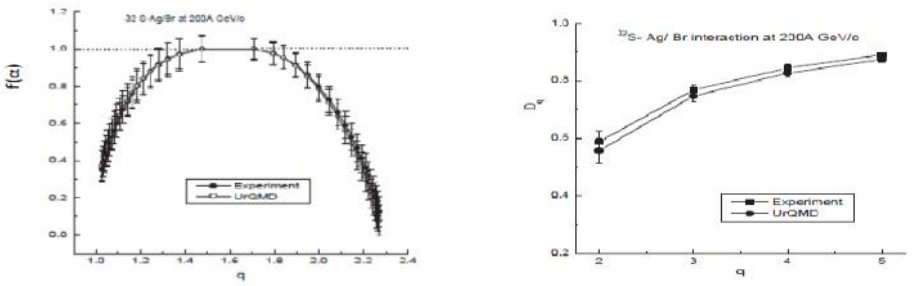

Figure 10: Left Panel: Multifractal Spectrum Function $f(\sim)$ for both Experiment and UrQMD. The Straight line Represents $f(\sim)=\sim$. Right Panel: Generalized Fractal Dimension D_q as a Function of q for both Experiment and UrQMD in Case of ^{32}S - Ag/Br Interaction.

The region above the line $f(\sim) = \sim$ corresponds to an unphysical region. The fact that a wide distribution in $f(\sim)$ and not a delta function peaked around $\sim_0$ has not been obtained. In the present analysis the peak values of the spectra are shifted to a higher value of $\sim$. All observations confirm the multifractal nature of the density fluctuation in each case. The left and right side of the spectrum corresponds, respectively, to the dense and sparse regions of density distribution. Both simulated and experimental maximum values of $f(\sim)$ are very close to unity, indicating that the empty bin effect particularly in higher resolution region, is marginal in the present case. The generalized fractal dimension D_q plotted against the order q in Fig. 10, the values of generalized fractal dimensions D_q determined using MFDFA methods are as follows:

Table 1

Interactions	q	Experiment		UrQMD	
		D_q	¢D_q	D_q	¢D_q
^{32}S - Ag/Br	**2**	0.437	0.0376	0.361	0.0440
	3	0.661	0.0178	0.601	0.0213
	4	0.752	0.0114	0.698	0.0139
	5	0.805	0.0083	0.753	0.0102

From the tabulated values of D_q obtained from the MFDFA method it clear that all values are much smaller than those obtained from the previous conventional methods. It is also clear from the tabulated values that there exists insignificant difference between the experimental values and the corresponding UrQMD predictions in case of ^{16}O - Ag/Br interactions, but there exists some discrepancies in case of ^{32}S - Ag/Br Interactions. In this present investigation a distinct and systematic increase in is found with the order number q. This behaviour is quite different from the behaviour in the D_q values obtained from the conventional methods. It should mention that the D_q values obtained from Takagi's method exhibit a sharp fall. This is probably because of the fact that Takagi moments are not free from the statistical noise [12].

4. DISCUSSION

In this analysis I presented a systematic analysis of the pseudorapidity fluctuation of charged mesons produced in ^{32}S - Ag/Br interaction at 200A GeV in terms of the Hwa's multifractal moments, Takagi's moments and DFA and MF-DFA methods. To understand the underlying mechanism(s) of particle production in these interactions, the experimental results are simulated by using the Fritiof model in case of first two moments and UrQMD model for the third technique. From the above analysis it is established that experimental data along with all simulated data behave like (multi)fractal system. The nature of $h(q)$,² (q) and the singularity spectra also confirm the presence of multifractality in the data as well as in the simulation. The nature of these spectra and the estimated values of the Hurst exponent H demand that the origin of fractality is of the two, three or higher order particle correlation in all cases. The MF-DFA prediction of the generalized fractal dimensions are consistently lower than that obtained from previous techniques like scale factorial moment analysis, Hwa's multifractal analysis and Takagi's method. In case of MFDFA moments it should noted that within the error margins the experimental results cannot be discriminated from their UrQMD values. The observations signify that the MFDFA technique like Hwa's multifractal moments and Takagi's moment is probably not sufficiently sensitive to the nature of fluctuation present in the data. A reliable method of filtering out the statistical noise from the MF-DFA function is needed to make the technique more effective.

5. ACKNOWLEDGEMENT

I am grateful to Professor P L Jain of SUNY at Buffalo, USA, and Professor Amithbha Mukhopadhyay, of University of North Bengal, West Bengal, India, respectively, for providing me the emulsion plates and allowing me to use the laboratory infrastructure. I am grateful to Dr. Prabhas Mali of University of North Bengal, West Bengal, India for helping me to run the computer code UrQMD and to generate the simulated data.

REFERENCES

1. *Hwa R C 1990 Phys. Rev. D **41** 1456*
2. *Florkowski W and Hwa R C 1991 Phys. Rev. D **43** 1548*
3. *Chiu C B and Hwa R C 1991 Phys. Rev. D **43** 100*
4. *Albajar C et al (UA1 Collaboration) 1991 Z. Phys. C **56** 37*
5. *Derado I, Hwa R C, Jansco G and Schmitz N 1991 Phys. Lett. B **283** 151*
6. *Shivpuri R K and Anand V 1994 Phys. Rev. D **50** 287*
7. *Sarkisyan E K, Gelovani L K and Taran G G 1993 Phys. Lett. B **302** 331*
8. *Adamovich M I et al (EMU01 Collaboration) 1998 Europhys. Lett. **44** 571*
9. *De Wolf E A, Dremin I M and Kittel W 1996 Phys. Rep. **270** 1*
10. *Ghosh M K, Mukhopadhyay A and Singh G 2006 J. Phys. G: Nucl. Part. Phys. . **34** (2007) 177–193*
11. *Hwa R C and Pan J 1992 Phys. Rev. D **45** 1476*
12. *Takagi F 1994 Phys. Rev. Lett. **72** 32*
13. *C.-K. Penget al., Phys. Rev. E 49 1685 (1994).*
14. *M.S. Taqquet al., Fractals 3 4, 785 (1995).*
15. *W. Kantelhardt et al., Physica A 316 87 (2002).*
16. *S.A. Bass, M. Belkacem, M. Bleicher, et al. Prog. Part. Nucl.Phys. 41, 255 (1998); M. Bleicher, E. Zabrodin, C. Spieles, et al. J. Phys. G, 25, 1859 (1999).*
17. *Anderson B, Gustavson G and Nilsson-Almqvist B 1987 Nucl. Phys. B **281** 289*
18. *Nilsson-Almquist B and Stenlund E 1987 Comput. Phys. Commun. **43** 387*
19. *Ghosh M K and Mukhopadhyay A 2003 Phys. Rev. C **68** 34907*
20. *Powell C F, Fowler P H and Perkins D H 1959 The Study of Elementary Particles by Photographic Method*
21. *(Oxford: Pergamon)*
22. *Bialas A and Gradzicki M 1990 Phys. Lett. B **252** 483*
23. *Brax Ph and Peschanski R 1991 Phys. Lett. B **253** 225*

24. *Ochs W 1990 Phys. Lett. B **247** 101,Ochs W 1991 Z. Phys. C **50** 339*
25. *Hentschel H G E and Proccacia I 1983 Physica D **40** 435*
26. *Bershadski A 1999 Phys. Rev. C **59** 364*
27. *Ghosh D et al 1997 Z. Phys. C **73** 269*
28. *Nayak S K and Viyogi Y P 1996 Phys. Lett. B **367** 386*
29. *J. Feder, Fractals, Plenum Press, New York, (1988).*
30. *H.-O. Peitgen, H. Jurgens, D. Saupe, Chaos and Fractals, Springer, New York, (1992), Appendix B.*